Nuclei Detection and Segmentation in Lung Histology

Noah Wagnon

Department of Electrical and Computer Engineering

The University of Alabama

Tuscaloosa, AL

ndwagnon@crimson.ua.edu

***Abstract*—Lung histology is the study of the microscopic structure of lung tissue images. With the rise of more efficient methods of obtaining histology images, there is an increased demand for accurate image processing techniques and algorithms to reliably analyze them and aid in the diagnosis of common lung ailments such as squamous-cell lung cancer (SSLC), lung adenocarcinoma, tuberculosis, pneumonia, and much more. Accurately detecting and segmenting nuclei is an excellent starting point for aiding such diagnoses. In this paper, we evaluate two approaches for performing detection and segmentation of lung cell nuclei. The first performs detection and segmentation simultaneously with a series of low-level image processing operations. The second utilizes a state-of-the-art deep learning network known as Mask- RCNN. This paper details each approach and offers a wholistic evaluation of the effectiveness of each.**

Keywords—nuclei, object detection, segmentation, lung histology, image processing, morphological operations.

I. Introduction

Lung histology imaging is one common clinical method for identifying and diagnosing lung ailments. These ailments commonly include tuberculosis, pneumonia, asthma, COPD, and lung cancer. Lung cancer is one of the most common and most deadly ailments. Lung cancer can come in a variety of forms including squamous cell carcinoma and adenocarcinoma. A trademark sign of cancerous tissue is an accelerated growth of cells along with their disfiguration and deviation from the typical round, uniform shape. Knowing this, pathologists can usually look for these signs to aid diagnosis. Unfortunately, manual clinical diagnoses can sometimes be inaccurate and incomplete.

The rise of advanced image processing techniques has opened the door for the use of automated tissue analysis as an aid to clinical diagnoses. For identifying cancerous tissues, a necessary, but challenging task is to accurately detect and segment all nuclei within a microscopic image. Automating the process of counting and displaying the shape of cell nuclei can be a tremendous help for pathologists. In this study, we evaluate two different approaches to this task. The first approach is to separate the detection and segmentation into two steps, each utilizing low-level image processing operations such as morphological openings, contrast enhancement, binarization, etc. The second approach is to utilize a common and powerful deep learning network known as Mask-RCNN.

Evaluation of each approach will be performed on the LC25000 dataset introduced later [1]. The deep learning model will be trained on the 2018 Data Science Bowl nuclei dataset [2]. This dataset contains multiple different stain types, but evaluation within this experiment will be limited to the common hematoxylin and eosin stain that generates pink and purple images.

II. Morphological detection Methodology

A. LC25000 Dataset

The LC25000 dataset contains 25,000 H&E-stained microscopic cell images. The breakdown of these images is as follows: 5,000 colon adenocarcinoma images, 5,000 benign colon images, 5,000 benign lung images, 5,000 squamous cell carcinoma images, and 5,000 lung adenocarcinoma images. Since this experiment is only interested in lung images, we neglect the colon cell images, leaving a dataset of 15,000 lung images each classified as benign, squamous cell, or adenocarcinoma. The dataset does not contain any masks or bounding box information. Figure 1 shows an example of an image from this dataset from the squamous cell carcinoma class.

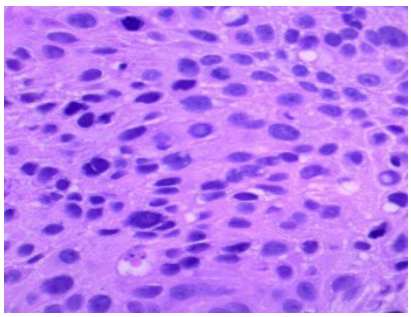

Figure 1. An example image from the LC25000 dataset.

B. *Contrast Enhancement via Top/Bottom-Hat Filtering*

Our goal for nuclei detection is to generate a single coordinate point that identifies the center of a nuclei. As seen in figure 1, a characteristic of the H&E stain style is that the background tissue is typically a light pink color while the nuclei themselves are a much darker purple. Our first step in generating these center points takes advantage of this H&E characteristic. We begin by converting the input image to grayscale and complementing it. The result is a grayscale image in which the purple nuclei regions are much brighter than the background tissue. Our algorithm interprets this brightness as the probability of a particular region being a nucleus.

We know for certain that our algorithm will utilize a binarization step. But before that step, we would benefit from an effective contrast enhancement to improve the binarization results. There are many effective options for contrast enhancement such as histogram equalization, but we ultimately decided to do to top/bottom-hat filtering for contrast enhancement.

A top-hat filtered image is computed by performing a morphological opening on the input image with a given structuring element. The resulting image is then subtracted from the original image to obtain the top-hat filtered output image. A bottom-hat filter computes a morphological closing of an input image and then subtracts the original image from the closing result to obtain the output.

In general, a top-hat filter causes bright regions in an image to appear brighter and dark regions to appear darker. A bottom-hat filter, in general, does the opposite. The result of subtracting a bottom-hat filtered image from a top-hat filtered image is a mask image that can be added to the original grayscale image to enhance the contrast. This is our selected preprocessing step, and we perform two iterations of this. The first uses a disk-shaped structuring element of size 30. The second iteration is the same process but with a structuring element of size 15. Figure 2 below shows this process from the original input to the preprocessed output. Note that we are using the image in figure 1 as input.

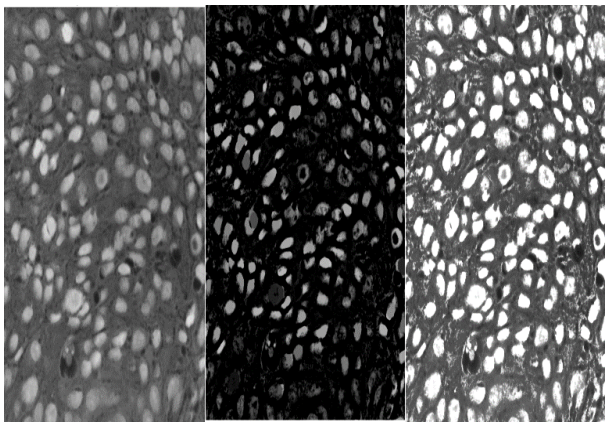

Figure 2. Left to Right: Grayscale and complemented input image, top-hat (-) bottom-hat filtered image, Addition of the first two images.

C. *Binarization and Morphological Opening*

With a contrast-enhanced input image shown in figure 2, we can now move on to binarizing this image as a middle step before completing the rest of the algorithm. For binarization, we are using Otsu's method. Otsu's method iteratively and dynamically selects a threshold value by iterating through possible threshold values and selecting the value that minimizes the foreground and background spread. After this value is selected, any pixel with intensity value below the threshold will be mapped to 0 (black) and all other pixels will be mapped to 1 (white). This result is shown on the left of figure 3.

We notice, however, that there are several minor debris left over after binarization. This is likely due to small patches remaining from the top and bottom hat filtering. We remove these small debris by performing a morphological opening utilizing a disk-shaped structuring element with a radius of size 5. The result of this step is shown on the right of figure 3.

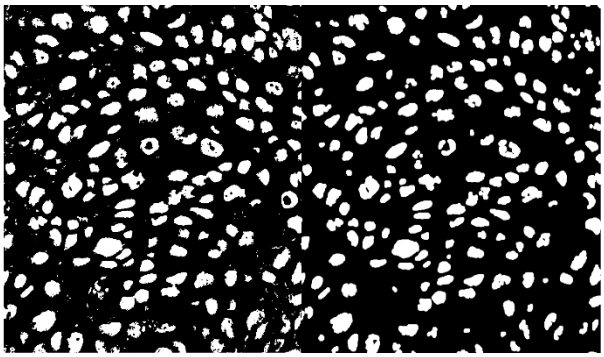

Figure 3. Binarization results (left) and opening results (right).

D. *Computing Center Points and Visualizing Detection Results.*

With the binarized image as computed in figure 3, the last step remaining is to analyze the distinct remaining connected components and compute their center region points. This is done by computing the perimeter of each connected component and inferring the center (x, y) coordinate. Since these center points are a size of 1 pixel, we perform a simple dilation on them to see the points more clearly. We can overlay the newly obtained center map on the original input to examine the detection results. This is shown in figure 4 below.

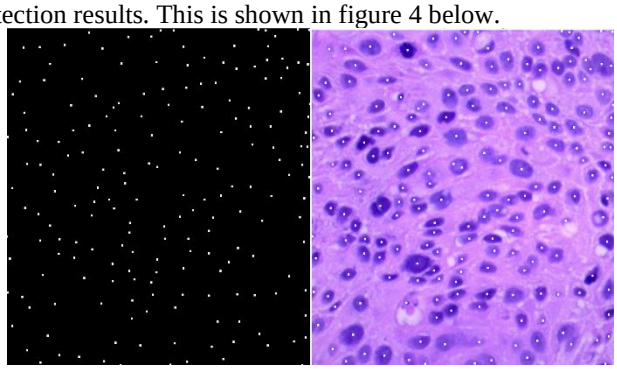

Figure 4. Center map (left) and detection results (right).

III. Morpholocial Segmentation Methodology

We can now turn our attention to proposing a separate algorithm to operate on the same input image simultaneously. This algorithm will perform segmentation of each nuclei instance. The steps for this algorithm are the exact same up until the morphological opening results shown in figure 3. After the opening, the segmentation algorithm performs its own steps for edge detection. We considered various other segmentation techniques such as watershed segmentation, but we ultimately settled on using a Laplacian of Gaussian (LoG) filter for edge detection.

A. Edge Detection via a Laplacian of Gaussian Filter

After obtaining a relatively clean, binarized image via a morphological opening shown in figure 3, we are now ready to apply our LoG filter. A Laplacian filter is a second derivative-based filter that is used to detect edges. Laplacian filters are often sensitive to noise, so a natural preprocessing step is to perform Gaussian smoothing to the input image before performing Laplacian filtering. These two steps can be combined into one filter and generate a convolution kernel. This mechanism is called a Laplacian of Gaussian filter, and the results are quite effective for our nuclei images. The results are shown below in figure 5.

After completing the Laplacian of Gaussian filtering and obtaining the results in figure 5, we can overlay the edges on the original input image to get a good visualization of our segmentation results. This is shown in figure 6.

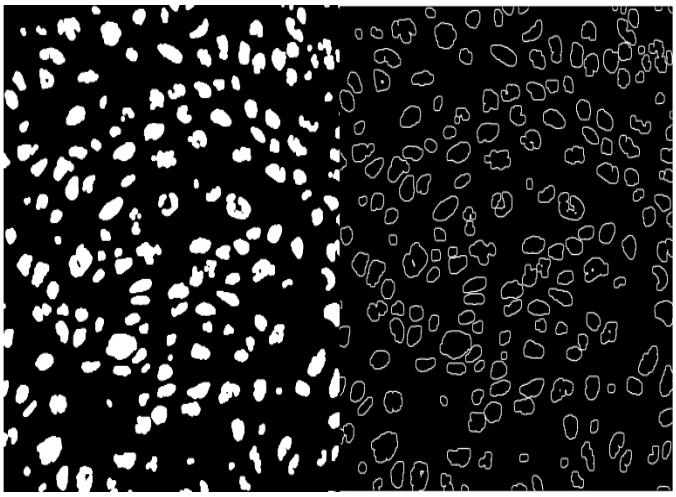

Figure 5. Binarized and Opened Image (left) and Results of LoG filtering (right).

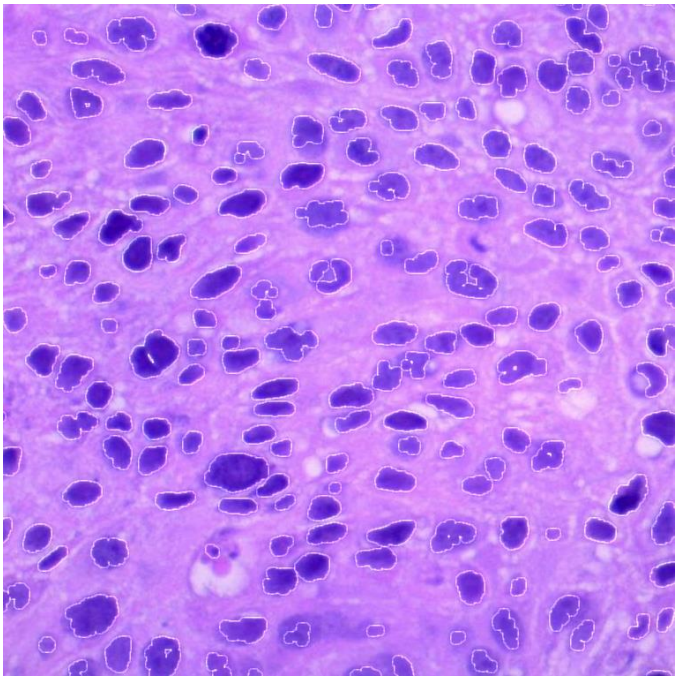

Figure 6. Input image with segmentation lines around nuclei.

IV. Deep Learning Approach Methodology

A. Neural Network and Dataset Used

Our deep learning-based approach for detecting and segmenting individual lung cell nuclei utilizes the popular deep neural network known as Mask-RCNN [3]. Mask-RCNN is an extension of popular object detection networks such as Faster-RCNN. Mask-RCNN extends these networks by not only offering bounding boxes and classification, but also offering segmentation masks for each object detected, making it the ideal neural network to train for this task since both detection and segmentation are crucial for determining nuclei count and structure.

With our network selected, we now need to select a dataset to train the network on. A common problem for deep-learning-based medical image tasks is dealing with the lack of datasets containing reliable ground truth data. Manually labeling these images can take an unreasonable amount of time, especially when considering that the labeler usually must be technically and clinically competent enough to confidently identify individual nuclei. We can imagine that an image such as figure 1 could take several minutes to accurately label. To train a model appropriately, we need at least a few hundred images and preferably much more.

Fortunately, a dataset exists with a reasonable amount of ground truth masks for individual nuclei [2]. The 2018 Data Science Bowl Kaggle dataset contains 37,333 annotated nuclei within 841 images. These 841 images are split within 5 different stain types. While the least common stain type within the dataset is the H&E stain that the LC25000 set uses, we still predict that our trained nuclei detector will perform well on the pink and purple LC25000 images [1].

B. *Training Procedure*

With the dataset and network selected, we turned our attention towards beginning the training procedure. We trained over 40 epochs using an 80/20 train/test split. The first 20 epochs will train just the heads and the last 20 epochs will train all layers. Train time took approximately 52 minutes using a single RTX6000 GPU. We used basic train-time augmentation techniques such as flips, rotations, and blur addition. We defined our training loss function as the sum of mask, class, and bounding box losses. Our training characteristic plot is shown below in figure 7. Our training and validation loss values bottomed out at 0.5411 and 0.9500, respectively. Our class, box, and mask losses bottomed out at 0.1091, 0.0793, and 0.1936, respectively.

Figure 7. Training Loss Plots.

C. *Deep Learning Output on LC2500 Input*

Our decision to train the model on the Data Science Bowl dataset was predicated on the prediction that the trained model would migrate nicely to the LC2500 dataset and perform accurate detection and segmentation on input images such as figure 1. Figure 8 below shows the output produced when figure 1 is fed to the model.

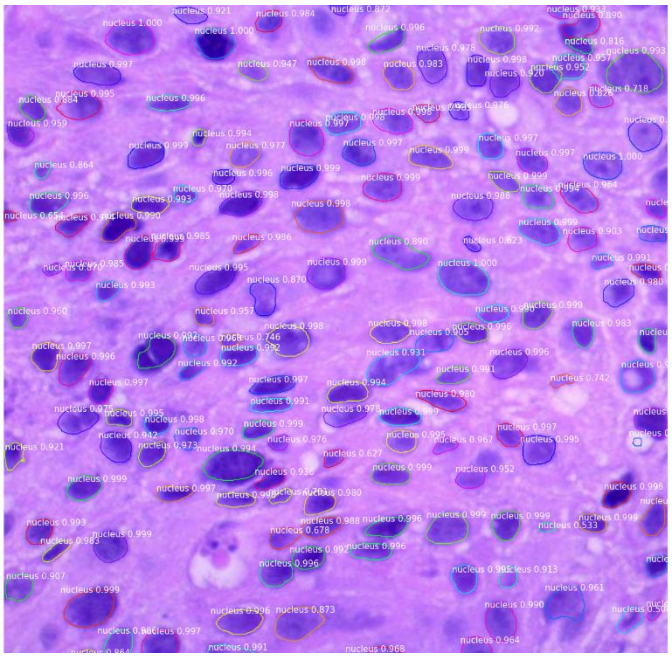

Figure 8. Example Model Output.

V. Results and Comparison of Two Approaches

A. *Results Using SCLC (Figure 1) Example.*

Most of our testing was performed on small-cell lung carcinoma (SCLC) images such as the example shown in figure 1. Figures 4 and 6 show the morphological approach's detection and segmentation results, while figure 8 shows the deep learning approach's results. To evaluate, we counted the number of nuclei present in figure 1. We then manually counted the number of true positives, false positives, and false negatives for both methods to create the confusion matrices shown below in figure 9.

175 true positives	11 false negatives
7 false positives	N/A (No true negative info)

160 true positives	25 false negatives
1 false positive	N/A (No true negative info)

Figure 9. Morphological approach confusion matrix (left) and deep learning approach confusion matrix (right).

Using the confusion matrix above, we found the accuracy, precision, F1 score, and the recall of the morphological approach to be 90.67%, 96.15%, 0.9511, and 94.09%, respectively. Likewise, we found the accuracy, precision, F1 score, and recall of the deep learning approach to be 86.02%, 99.38%, 0.9249, and 86.49%, respectively.

We can see that the deep learning approach has a higher precision, meaning that it has a lower false positive rate. On the other hand, we can see that the morphological approach had a higher recall, implying a lower false negative rate. There is always a tradeoff between recall and precision, but in this application, precision is more important since false positives can be detrimental to aiding diagnoses. In this sense, the deep learning approach gets a slight edge as far as quantitative results.

B. *Testing on Normal Lung Tissue and Adenocarcinoma tissue*

All our figures so far have used SCLC examples. Both methods performed well on SCLC images. We found that the morphological approach performed very well on normal lung images but struggled a bit on adenocarcinoma images. On the contrary, the deep learning approach performed well on the adenocarcinoma examples while struggling on the normal lung tissue. In figure 10 we will present an example of the morphological approach on normal lung tissue and the deep learning approach on an adenocarcinoma image.

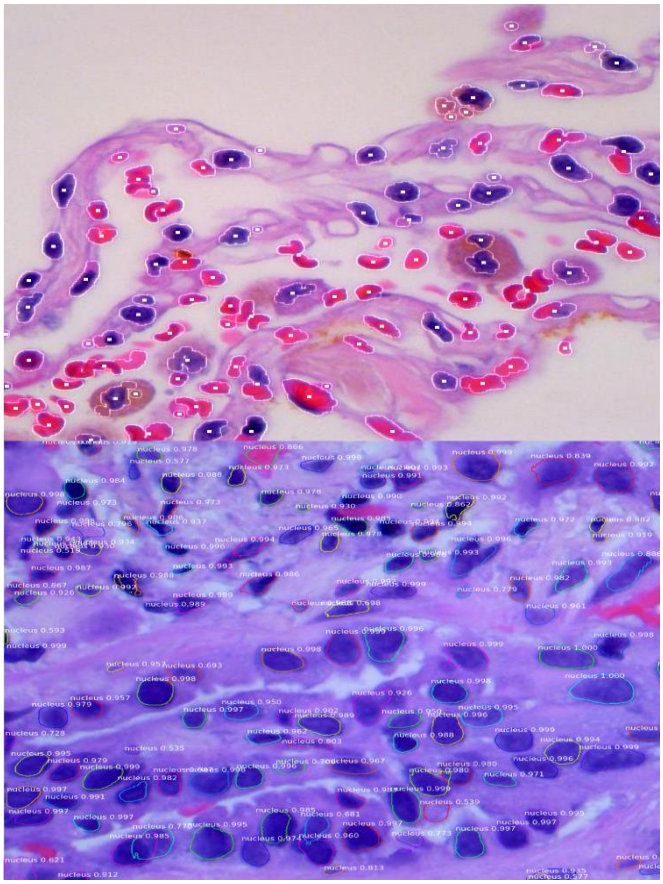

Figure 10. Normal lung tissue with morphological approach (top) and adenocarcinoma tissue with deep learning approach (bottom).

C. *Overall Comparison of the two Approaches*

While performance seems to be nearly the same in this small experiment, the deep learning approach has much more potential to become more robust in the future. The main problem is the shortage of ground truth image sets for nuclei detection, although recent work has shown that utilizing a Generative Adversarial Network (GAN) to automatically create synthetic tissue images with ground truth can effectively tackle this issue [4]. This would certainly be a worthwhile addition to any future work on this project. The deep learning approach also has a slight advantage when it comes to segmentation accuracy and full bounding box and mask info. Furthermore, the deep learning approach can generalize to many different stain types. Despite having limitations, the morphological approach performed surprisingly well. It is worth noting that the morphological approach is much less computationally expensive and requires much less overhead.

VI. Conclusion

In this paper we have proposed and compared two solutions to the problem of nuclei detection and segmentation in microscopic lung histology images. The first method uses a series of low-level, morphological-based image processing techniques and filters to perform detection and segmentation. Evaluation showed that this method had high recall (94.09%) but the precision was slightly lower (96.15%) than our other method due to several false positives. We also proposed a deep learning-based method that utilizes Mask-RCNN network trained on the 2018 Data Science Bowl dataset containing ground truth masks and bounding boxes for nuclei with 5 different stain types. Performance overall was similar between the two methods. The deep learning approach resulted in a lower recall of (86.49%) but a very high precision (99.38%). Due to false positives being more detrimental than false negatives in pathological analysis, we value the precision results more than the recall, giving our deep learning approach a slight edge.

The quantitative results are promising so far, but the main issue keeping our deep learning approach from being as robust as possible is the lack of ground truth data outside of the Data Science Bowl dataset. In the future we look to pursue using a GAN to generate synthetic ground truth images to diversify our training data and evaluation methodology [4]. If these additions work well, our proposed solution could be a very useful tool for pathologists attempting to identify nuclei and judge their shape when looking for cancerous tissue.

REFERENCES

[1] Borkowski AA, Bui MM, Thomas LB, Wilson CP, DeLand LA, Mastorides SM. "Lung and Colon Cancer Histopathological Image Dataset"(LC25000).[Dataset]. Available: https://www.kaggle.com/andrewmvd/lung-and-colon-cancer-histopathological-images

[2] Caicedo, J.C., Goodman, A., Karhohs, K.W. *et al.* Nucleus segmentation across imaging experiments: the 2018 Data Science Bowl. *Nat Methods* **16,** 1247–1253 (2019). https://doi.org/10.1038/s41592-019-0612-7

[3] K. He, G. Gkioxari, P. Dollár and R. B. Girshick, "Mask R-CNN", *CoRR*, 2017.

[4] S. Lee, C. Fu, P. Salama, K. W. Dunn, and E. J. Delp, "Tubule segmentation of fluorescence microscopy images based on convolutional neural networks with inhomogeneity correction," Proceedings of the IS&T International Symposium on Electronic Imaging, vol. 2018, no. 15, pp. 199–1–199–8, January 2018, Burlingame, CA.